Analytical Methods

ROYAL SOCIETY OF CHEMISTRY

PAPER

View Article Online
View Journal | View Issue

Cite this: *Anal. Methods*, 2025, **17**, 2467

Development and validation of a novel UV-TOF MS method for real-time exhaled propofol analysis in Beagles†

Pan Chang,‡[ad] Xiaoxiao Li,‡[ad] Xing Liu,[d] Yi Kang,[d] Deying Gong,[d] Wenwen Li,[b] Zhongjun Zhao,[c] Tao Zhu,[ad] Jin Liu[ad] and Wen-sheng Zhang *[ad]

Propofol, a fast-acting anesthetic, requires precise titration to minimize adverse effects. While plasma-based monitoring is slow, exhaled propofol offers a real-time, non-invasive alternative, though its clinical application remains limited. This study evaluates ultraviolet time-of-flight mass spectrometry (UV-TOF MS) for real-time monitoring, presenting its calibration and validation in Beagle dogs. Calibration showed excellent linearity (R^2 = 0.9939) over 3.23–46.13 ppbv. The intra-day imprecision at propofol concentrations of 4.61 and 23.06 ppbv was below 5.83% and 7.75%, respectively, while the inter-day imprecision was 9.69% and 9.75%, respectively. Carry-over effects were minimal, with signal recovery within 40–60 s, measuring 8.7%, 9.1%, and 4.7% at 4.61, 9.30, and 23.06 ppbv, respectively. In Beagle dogs, $C_{exhaled}$ exhibited a moderately strong linear correlation with C_{plasma} (R^2 = 0.7950) and a moderate correlation with sedative effects, as indicated by the bispectral index (R^2 = 0.5501) after a single bolus injection. Pharmacokinetic (PK) analysis revealed a delay in peak concentration (T_{max}) for $C_{exhaled}$ (2.00 ± 0.21 min) compared to C_{plasma} (1.00 ± 0.00 min). While AUC values were not directly comparable, both exhibited R_AUC > 80%, indicating reliable drug kinetic reflection. Mean residence time (MRT) and elimination rate constants (λ_z) showed no significant differences. These results suggest that exhaled breath analysis provides pharmacokinetic insights comparable to plasma, with a slight delay in peak concentration. UV-TOF MS proved to be an efficient method for detecting exhaled propofol, offering potential for real-time anesthesia monitoring in clinical settings.

Received 24th November 2024
Accepted 22nd February 2025

DOI: 10.1039/d4ay02131b

rsc.li/methods

1 Introduction

Propofol is a widely used anesthetic known for its rapid onset and short duration of action, making it ideal for inducing and maintaining anesthesia during surgery.[1,2] Administered intravenously by qualified physicians, its dosage is tailored to factors such as the patient's age, weight, medical history, and the procedure being performed.[3,4] Despite its efficacy, propofol is associated with side effects, including hypotension,[5] respiratory depression,[6,7] electroencephalogram (EEG) burst suppression,[8] intraoperative awareness,[9] and, in severe cases, propofol infusion syndrome.[10] Thus, enhancing the precision of propofol titration in clinical anesthesia remains crucial.

The traditional method for monitoring propofol concentration relies on plasma measurement using liquid chromatography-mass spectrometry. However, this approach is offline, time-consuming, and requires bulky, expensive equipment, making it unsuitable for point-of-care applications.[11] Recent studies have explored the detection of propofol in exhaled breath, highlighting the potential of online monitoring to significantly improve time resolution for drug detection. These studies demonstrated strong correlations between propofol concentrations in exhaled air, brain tissue, and plasma.[12–14] Real-time monitoring of exhaled propofol could address the need for maintaining effective dosing, enabling more precise and personalized patient care, particularly during total intravenous anesthesia.[15]

There is still a lack of effective techniques for real-time monitoring of propofol. Key factors for online monitoring of exhaled drugs include sensitivity, selectivity, sampling speed, and robustness. Exhaled target molecules must be ionized and separated in the gas phase by a mass analyzer. To address this, our team has developed a novel online mass spectrometer that integrates ultraviolet (UV) ionization with time-of-flight mass

[a]*Department of Anesthesiology, West China Hospital, Sichuan University, Chengdu, China. E-mail: zhang_ws@scu.edu.cn*

[b]*West China School of Public Health and West China Fourth Hospital, Sichuan University, Chengdu, China*

[c]*School of Mechanical Engineering, Sichuan University, Chengdu, China*

[d]*Laboratory of Anesthesia and Critical Care Medicine, National-Local Joint Engineering Research Centre of Translational Medicine of Anesthesiology, West China Hospital, Sichuan University, Chengdu, China*

† Electronic supplementary information (ESI) available. See DOI: https://doi.org/10.1039/d4ay02131b

‡ Pan Chang and Xiaoxiao Li contributed equally to this study.

spectrometry (TOF MS). UV photoionization, a soft ionization technique, excites molecules to a high-energy state where they absorb photons and become ionized, producing charged ions with minimal fragmentation.[16,17] The system completes ionization and detection of all volatile organic compounds (VOCs) within 0.1 s, significantly reducing analysis time and enabling real-time monitoring. UV-TOF MS also facilitates high-throughput, comprehensive tracing of gaseous VOCs,[18] effectively identifying isomers and rapidly generating visual spectra, providing anesthesiologists with quick and visualized results.

To address the limitations of plasma-based propofol monitoring, this study aims to develop and validate a real-time, non-invasive method for exhaled propofol detection using ultraviolet time-of-flight mass spectrometry (UV-TOF MS). The UV-TOF MS system (Aliben Science & Technology Co., Ltd, Chengdu, China) comprises key components, including a UV photoionization chamber, a radiofrequency multipole ion guide, electrostatic lenses, and a TOF mass analyzer. The system operates at a vacuum pressure of 500 ± 20 Pa maintained by a pump. By integrating UV photoionization with high-resolution mass spectrometry, this system enables rapid and efficient ionization of volatile organic compounds with minimal fragmentation. A key innovation is the incorporation of a fully automated reference gas generator for calibration, ensuring accurate quantification of exhaled propofol. Through a series of validation experiments and pharmacokinetic analysis in Beagle dogs, this study evaluates the feasibility, precision, and reliability of UV-TOF MS for real-time breath analysis, offering potential applications in clinical anesthesia monitoring.

2 Materials and methods

2.1. Chemicals

Propofol (purity: 99.0%) was purchased from Shanghai yuanye Bio-Technology Co., Ltd (China), and thymol was purchased from Fisher International Company (Fisher, USA). High-performance liquid chromatography (HPLC)-grade acetonitrile and methanol were purchased from Fisher International Company (Fisher, USA). High-purity (99.99%) nitrogen gas (N_2) was obtained from the gas supply center of our laboratory at West China Hospital, Sichuan University, Chengdu, China. Ultrapure water was obtained using a Milli-Q® integral water purification system (Merck Millipore, Darmstadt, Germany).

2.2. UV-TOF MS instrumentation and the working principle

When analyzing a sample gas, the sampling bag or the distal end of a gas tube is connected to the sampling tube of the UV-TOF MS. A negative pressure flow rate of 70 mL min^{-1} within the tube continuously introduces the sample gas into the ion source. A direct current krypton lamp emits photons with an energy of 10.6 eV, instantly ionizing organic compounds with ionization energies below this threshold. The ionized molecules are guided through the radiofrequency multipole and directed into the electrostatic lens setup. The ions are then separated in a field-free region by the mass analyzer based on their time of flight to the detector. The system measures mass-to-charge (m/z) ratios ranging from 10 to 455, with a signal acquisition time of 20 s. The detailed system parameters are listed in Appendix A, Table S1.†

2.3. Parameters for the gas generator

The standard gas generator system (Fig. 1) consists of a storage chamber containing a standard aqueous propofol solution, regulated by a liquid flowmeter (0–2 g h^{-1}). Pure N_2, adjusted with a gas flowmeter (0–1000 mL min^{-1}), merges with the aqueous solution in a vaporizer, where both components are heated to 100 °C, producing standard gaseous propofol with 100% relative humidity. The standard gas is then introduced into the detection system of the UV-TOF MS by a sampling inlet at a negative pressure flow rate of −70 mL min^{-1}. To ensure a consistent dilution ratio and minimize flowmeter errors, the liquid flowmeter was set to 0.8 g h^{-1}, and the gas flowmeter was fixed at 800 mL min^{-1}.

2.3.1. Calibration of the concentration of standard gaseous propofol. First, assume the liquid flowmeter parameter (g h^{-1}) to be X. Using the ideal gas law, expressed as "$pV = nRT$", the mass flow rate of the aqueous solution (g h^{-1}) can be converted to the volume flow rate (mL min^{-1}) as shown in eqn (1).

$$V_1 = nRT \div p = (X \div 18) \times RT \div (p \times 60) \quad (1)$$

where V_1 is the flow rate (mL min^{-1}), n is the amount of water (mol), R is the gas constant (8.314), T is the temperature (°C), and p is the atmospheric pressure in pascal (Pa).

Second, the original stock solution after gasification is defined as the standard propofol gas and the concentration C_0 (parts per billion by volume, ppbv) can be calculated according to eqn (2),

$$C_0 = \frac{m_1}{M_1} \times \frac{M_2}{m_2} \times 10^9 \quad (2)$$

where m_1 is the mass of propofol gas (g), M_1 is the molar mass of propofol gas (g mol^{-1}), m_2 is the mass of water (g), and M_2 is the molar mass of water (g mol^{-1}).

Finally, the actual bulk concentration of standard gaseous propofol (C_n) was calculated using a dilution ratio according to eqn (3).

$$C_n = V_1/V_{N_2} \times C_0 \quad (3)$$

where V_1 is the flow rate (mL min^{-1}) of the liquid flowmeter, V_{N_2} is the flow rate (mL min^{-1}) of the gas flowmeter for N_2, and C_0 is the nominal concentration of propofol in the stock room (ppbv).

2.3.2. The dilution protocol for the standard working solution of propofol. Propofol has limited water solubility (124 mg L^{-1}), much lower than its solubility in alcohol or toluene.[19] Despite this, aqueous stock solutions of propofol were prepared at concentrations below 124 mg L^{-1}. A stock solution (96.2 mg L^{-1}) was created by dissolving 5 μL of propofol standard in 50 mL of HPLC-grade water using ultrasound-assisted dissolution for 30 min and stored at room temperature. Despite the low solubility of propofol, the concentration of propofol in the stock solution (96.2 mg L^{-1}) was significantly

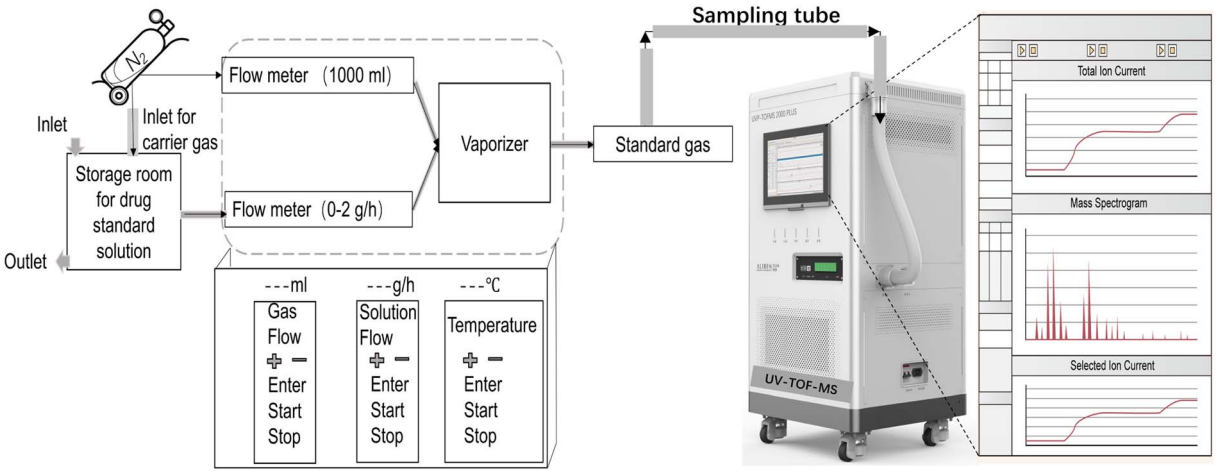

Fig. 1 Schematic experimental setup of the gas generator and UV-TOF MS detection system.

lower than its intrinsic solubility (124 mg L^{-1}), ensuring complete dissolution. Additionally, the stock solution was ultrasonically mixed before each use, ensuring its stability.

The nominal concentration of propofol in the stock solution was calculated as 9713 ppbv using eqn (2). Standard working solutions with nominal concentrations of 3.23, 4.61, 6.92, 9.23, 23.06, and 46.13 ppbv were prepared by serially diluting the stock solution in HPLC-grade pure water, as detailed in Appendix A, Table S2.† Gradients of propofol standard gas were then generated from these working solutions following the method described in Section 2.3. Each concentration of propofol standard gas was continuously monitored for at least 10 minutes, with a signal acquisition interval of 20 s.

2.4. Method validation

2.4.1. Selectivity. The characteristic spectral peak of propofol was identified in two steps. First, the propofol standard (purity: 99.0%) was heated to 60 °C, and the headspace air was analyzed using the UV-TOF MS system to detect the *m*/*z* value with a significant increase in signal intensity, which was identified as the target signal of propofol. Second, standard gaseous propofol at gradient concentrations was collected through sampling tube and analyzed by UV-TOF MS. A distinct signal peak, whose intensity increased proportionally with the gradient concentrations of propofol standard gas, was detected at a consistent *m*/*z* value and confirmed as the characteristic peak of propofol.

2.4.2. Calibration curve. A six-point calibration curve was established using diluted propofol standard solutions at nominal concentrations of 3.23, 4.61, 6.92, 9.23, 23.06, and 46.13 ppbv. The UV-TOF MS signal intensity stabilized, confirming its correlation with the nominal propofol concentrations.

2.4.3. Carry-over effect. Nominal concentrations of 4.61, 9.23, and 23.06 ppbv were maintained for at least 10 consecutive data points after reaching a stable signal intensity before changing the concentration to 0 ppbv (pure air). The signal intensity was then monitored to assess the time taken for the propofol signal to decline and the extent of its decline.

2.4.4. Inter-day and intra-day imprecisions. Intra-day and inter-day imprecisions were evaluated at two quality control (QC) levels using standard gaseous propofol at 9.23 and 23.06 ppbv. The gas generator continuously produced standard gas, which was analyzed with the UV-TOF MS system over three consecutive days. Imprecision was calculated as the relative standard deviation (RSD), expressed as a percentage of the mean measured value, based on at least 15 repeated measurements. An RSD within ±15% was considered acceptable.

2.5. Animal experiments

The study protocol was approved by the Institutional Animal Care and Use Committee of West China Hospital, Sichuan University, Chengdu, China (Approval No. 20220420001). Six male Beagle dogs (1–1.5 years old, 9–13 kg, DOSSY Experimental Animals Co. Ltd, Chengdu, China) were included. Subjects fasted for 8 hours before the experiment. Bilateral forelimb veins were catheterized for drug administration and blood sampling. Blood samples (0.3 mL) were collected at 1, 3, 5, 7, 10, 20, and 30 min after propofol injection, using ethylenediaminetetraacetic acid anticoagulant tubes, and then centrifuged at 3500 rpm for 10 min at 4 °C. A 100 μL supernatant was stored at −80 °C for HPLC analysis.

EEGs were recorded to evaluate anesthesia, with BIS values calculated over the temporal-frontal area every 20 s. Anesthesia induction was achieved with tiletamine–zolazepam (Zoletil®50, Virbac, France, 5 mg kg^{-1}). The dogs were tracheally intubated and mechanically ventilated with pure oxygen, maintaining a tidal volume of 10 mL kg^{-1}, a respiratory rate of 20 breaths per min, an inspiratory-to-expiratory ratio of 1 : 2, and end-tidal CO_2 at 30–40 mm Hg. A single 5 mg per kg bolus of propofol, twice the ED50 for loss of the righting reflex in Beagles, was administered over 5 s. Body temperature was maintained at 36.5 °C ± 0.5 °C. Upon recovery, the endotracheal tube and catheters were removed, and the dogs were returned to the breeding room after full recovery.

Exhaled breath was collected *via* the UV-TOF MS system, using a polytetrafluoroethylene tracheal tube connected by a polycarbonate three-way valve. The *m*/*z* 178 mass peak was selected for propofol detection, with signal intensity monitored every 20 s. Data collection started immediately after propofol administration and ceased once spontaneous respiration resumed. The propofol concentrations were calculated using calibration curves.

2.6. HPLC to determine the plasma concentration of propofol

A selective and sensitive HPLC method with fluorometric detection was developed to measure plasma propofol concentrations. The analysis was performed on a Waters 2695 HPLC System with a Waters 2475 fluorescence detector (Waters, US) using a SWELL C18 column (150 × 4.6 mm, 5 μm). The mobile phase, a mixture of acetonitrile and water (62 : 38, v/v), was delivered at a flow rate of 1.0 mL min^{-1}. Excitation and emission wavelengths were set at 276 nm and 310 nm, respectively.

The retention times were 7.4 min for propofol and 3.9 min for thymol (internal standard). The propofol standard solution was prepared by dissolving 20 mg of propofol reference substance in methanol to a final concentration of 2.0 mg mL^{-1} and stored at 4 °C. Before use, the stock solution was diluted with methanol to prepare working solutions with concentrations of 48.87, 97.73, 293.19, 879.58, 2638.75, 7916.25, 10 555.00, and 21 110.00 ng mL^{-1}. The internal standard solution was made by dissolving 10 mg of thymol in methanol to a concentration of 1.0 mg mL^{-1}, and then diluted with acetonitrile to create a working solution of 500 ng mL^{-1}. For sample preparation, 50 μL of plasma was mixed with 200 μL of the internal standard working solution in an Eppendorf tube, vortexed for 1 min, and centrifuged at 20 000 rpm at 4 °C for 10 min. A 10 μL aliquot of the supernatant was then injected for analysis.

For the determination of propofol concentration in plasma by HPLC, an eight-point calibration curve was established by taking 45 μL blank plasma and adding 5 μL standard series working solutions to produce plasma propofol concentrations of 48.87, 97.73, 293.19, 879.58, 2638.75, 7916.25, 10 555.00, and 21 110.00 ng mL^{-1}. Then, the samples were processed according to the method described above in Section 2.3.2 and analyzed. The standard curve was established using the ratio of the peak area of propofol to the internal standard on the *y*-axis and the plasma concentration of propofol on the *x*-axis. Weighted regression ($1/x^2$) was performed to obtain a regression equation of $y = 0.000062x - 0.000104$ ($r = 0.999$). The linearity was within the range of 48.9 and 21 110.0 ng mL^{-1}.

To determine plasma propofol concentrations by HPLC, an eight-point calibration curve was created by mixing 45 μL of blank plasma with 5 μL of standard working solutions to achieve final concentrations of 48.87, 97.73, 293.19, 879.58, 2638.75, 7916.25, 10 555.00, and 21 110.00 ng mL^{-1}. The samples were prepared as described in Section 2.3.2 and analyzed. The calibration curve was constructed by plotting the ratio of propofol to internal standard peak areas (*y*-axis) against plasma propofol concentrations (*x*-axis). Weighted regression ($1/x^2$) yielded the equation $y = 0.000062x - 0.000104$ with $r = 0.999$, showing linearity in the range of 48.9 to 21 110.0 ng mL^{-1}.

2.7. Statistical analysis

The mass spectrum, which displays the signal intensities of ions with specific *m*/*z* values, was generated synchronously using the UV-TOF MS data display system. Statistical analyses were performed using Microsoft Excel and GraphPad Prism 9.0 (GraphPad Software, San Diego, CA, US). The normality of the data was assessed using the Shapiro–Wilk test. Pairwise comparisons were performed using *t*-tests. Nonparametric comparisons were conducted using the Mann–Whitney test. Linear regression was used to create the calibration curves. Statistical significance was defined as $P < 0.05$. For the pharmacokinetic (PK) studies of propofol in both plasma and exhaled air, the PK parameters were analyzed by the non-compartment method using DAS 3.3.0 (Shanghai, China).

When calculating PK parameters for propofol, to enhance the comparability between the exhaled concentration and plasma concentration, the exhaled concentration of propofol was converted into mass concentration based on the ideal gas law. Subsequently, PK parameters were computed using DAS 3.0 and the NCA (non-compartmental analysis) model was applied for PK modeling.

3 Results

3.1. Validation of the UV-TOF MS method

3.1.1. Selectivity. Introducing the propofol gaseous standard into the analysis system resulted in a marked increase in the peak height at *m*/*z* 178, corresponding to propofol's molecular weight. This increase correlated with the increasing concentrations of the gaseous standard and was accompanied by a significant rise in total ion current intensity. The instrument software provided detailed signal parameters, including the intensity, peak area, width, height, and spectrum. Fig. 2 illustrates the mass spectrum of the sample gas in the UV-TOF MS system, highlighting the *m*/*z* 178 peak at different propofol concentrations (0, 9, and 23 ppbv).

3.1.2. Calibration curves and the carry-over effect. Fig. 3A shows the calibration curves correlating UV-TOF MS signal intensity with nominal gaseous propofol concentrations (ppbv). Each concentration was measured at least 15 times after achieving a stable signal, represented by blue dots. Linear regression yielded $y = 19260x - 60117$ with $R^2 = 0.9939$, demonstrating strong linearity within the range of 3.23–46.13 ppbv.

Fig. 3B illustrates the carry-over effect, assessed by transitioning from sampling propofol concentrations (4.61, 9.23, and 23.06 ppbv) to pure air (0 ppbv). The signal returned to baseline within 20–40 s (1–2 measurements) after sampling stopped. Carry-over effects were quantified as 4.7%, 9.1%, and 8.7% for concentrations of 23.06, 9.23, and 4.61 ppbv, respectively.

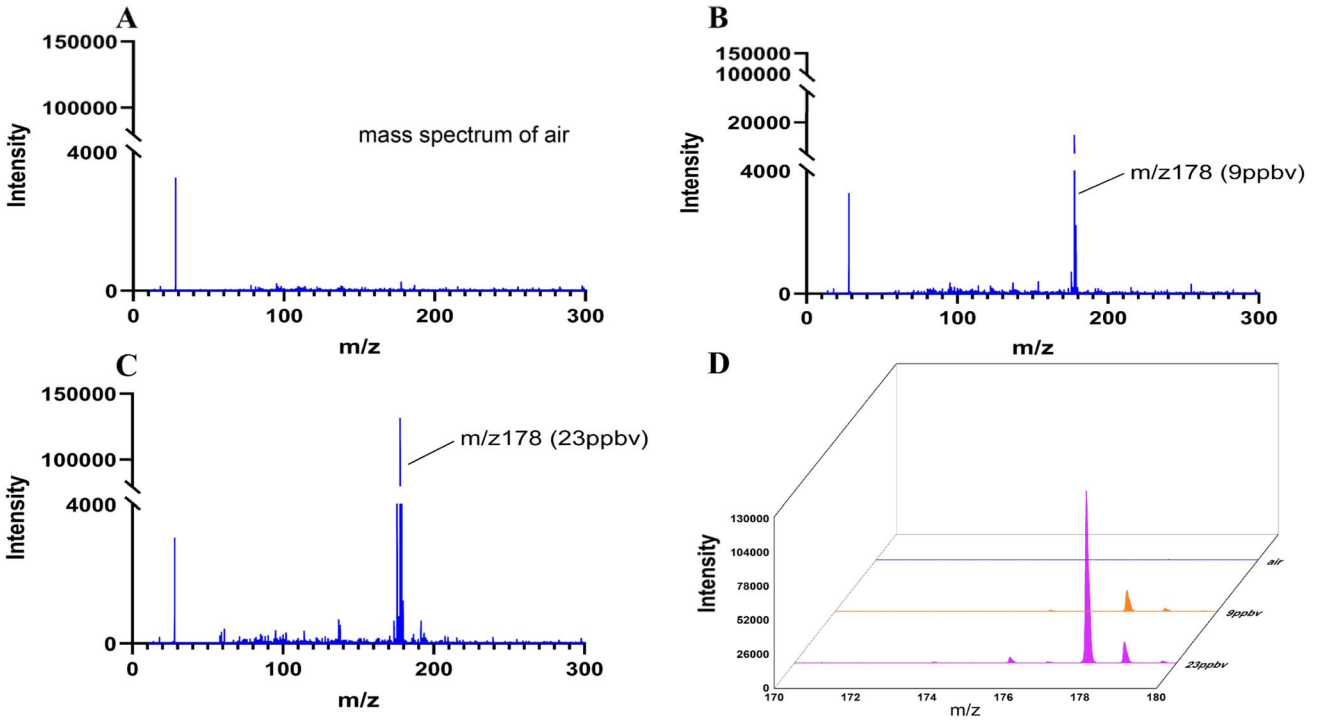

Fig. 2 The mass spectra of propofol (*m*/*z* 178) in the UV-TOF MS system. (A) Mass spectra of air. (B) Mass spectra with propofol at 9 ppbv. (C) Mass spectra with propofol at 23 ppbv. (D) Representation of *m*/*z* 178 intensity at different concentrations in a single coordinate system.

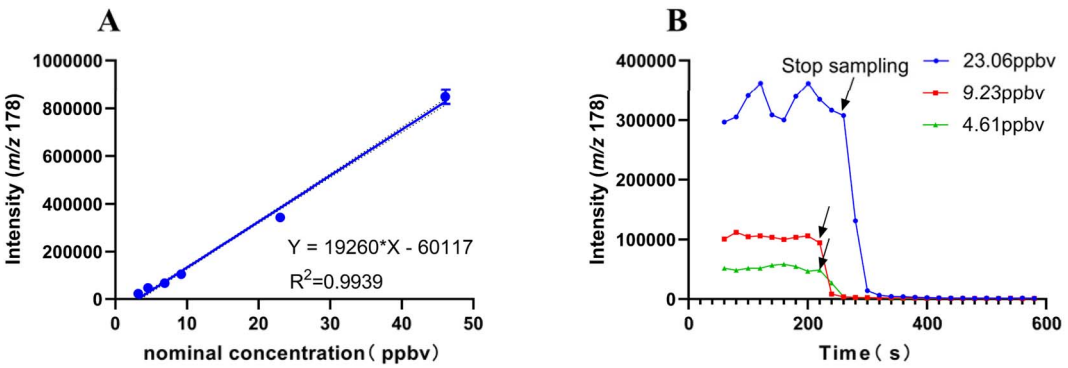

Fig. 3 The calibration curve and the carry-over effects of the UV-TOF MS system. (A) The measured values at each nominal concentration of propofol standard gas ($n = 15$) are shown as blue dots. A quadratic plot illustrates the relationship between UV-TOF MS signal intensity and gaseous propofol concentration (ppbv), with an R^2 value of 0.9939. (B) The carry-over effects of the UV-TOF MS system were assessed at gaseous propofol concentrations of 4.61, 9.23, and 23.06 ppbv. Standard gas sample collection ceased at the point marked by the black arrow.

Table 1 Intra- and inter-day imprecision of the assay[a]

	Intra-day ($n = 15$)		Inter-day ($n = 15$)	
NC	MI	RSD (%)	MI	RSD (%)
4.61 ppb	42 634	5.83	43 393	9.69
	51 195	5.31	42 741	3.62
	50 522	4.20	52 180	7.25
23.06 ppb	331 061	6.51	312 621	5.30
	325 625	7.75	315 607	7.57
	308 585	4.98	313 514	9.75

[a] NC: nominal concentration of propofol standard gas. MI: measured intensity.

3.1.3. Inter-day and intra-day imprecisions. Intra-day and inter-day imprecisions were evaluated at two concentrations (4.61 and 23.06 ppbv), with results summarized in Table 1. The RSD was below 5.83% and 7.75% at 4.61 and 23.06 ppbv, respectively. The inter-day RSD was 9.69% and 9.75% for the same concentrations.

3.2. Animal experiments and PK study

3.2.1. Correlations between $C_{exhaled}$ and C_{plasma}, and $C_{exhaled}$ and BIS. The validated method was successfully applied for a PK study of propofol in six Beagles after intravenous

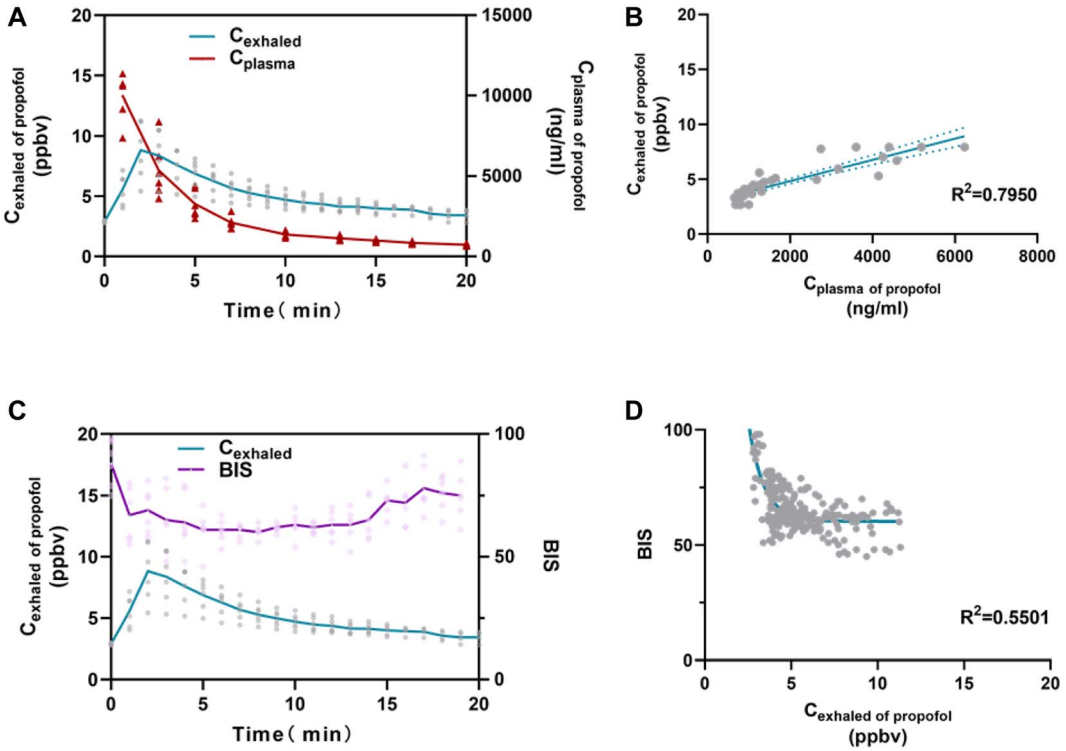

Fig. 4 Correlations between $C_{exhaled}$ and C_{plasma}, $C_{exhaled}$ and BIS. (A) Concentration–time profiles between $C_{exhaled}$ and C_{plasma} of propofol after intravenous injection in Beagles (mean ± SD, $n = 6$). (B) Linear correlation in $C_{exhaled}$ and C_{plasma} of propofol ($y = 17.12x + 9170.30$, $R^2 = 0.7950$, $P < 0.05$). (C) Time course of $C_{exhaled}$ and BIS (mean ± SD, $n = 6$). (D) Correlation between $C_{exhaled}$ of propofol and BIS follows a one-phase exponential decay model ($y = 220.41x^{-0.115}$, $R^2 = 0.5501$).

administration at a dosage of 5 mg kg^{-1}. The concentration–time profiles of propofol in exhaled air ($C_{exhaled}$) and plasma (C_{plasma}) are presented in Fig. 4. After administration, C_{plasma} increased rapidly, peaking at ~1 min, while $C_{exhaled}$ peaked at ~3 min. Both concentrations then declined in parallel. The BIS value dropped sharply, reaching its minimum at ~1 min, remained stable for 15 min, and then increased during the awakening phase. The exhaled propofol intensity was quantified using the linear calibration curve from Section 3.1.2. A linear relationship was observed between $C_{exhaled}$ and C_{plasma} ($y = 17.12x + 9170.30$, $R^2 = 0.7950$). Additionally, $C_{exhaled}$ and BIS values showed a moderate correlation, modeled by one-phase exponential decay ($y = 220.41x^{-0.115}$, $R^2 = 0.5501$) (Fig. 4).

3.2.2. The PK model and parameters of $C_{exhaled}$ and C_{plasma} after bolus injection. The main PK parameters of propofol were analyzed using a noncompartmental model in DAS 3.3.0

Table 2 The NCA pharmacokinetic parameters of propofol (5 mg kg^{-1}) after single intravenous administration in Beagles ($n = 6$)[a]

Parameters	Unit	$C_{exhaled}$	Unit	C_{plasma}	P (t-test)
AUC (0–t)	ppbv min	80.80 (21.28)	μg L^{-1} min^{-1}	60766.58 (16457.29)	—
AUC (0–∞)	ppbv min	89.12 (21.83)	μg L^{-1} min^{-1}	70240.43 (20904.37)	—
R_AUC (t/∞)	%	90.42 (7.36)	%	87.07 (2.83)	0.3029
AUMC (0–t)	min min ppbv	606.22 (170.88)	min min μg L^{-1}	294932.68 (118918.12)	—
AUMC (0–∞)	min min ppbv	909.61 (407.84)	min min μg L^{-1}	629359.52 (340053.99)	—
$T_{1/2z}$	min	8.11 (5.43)		9.02 (3.98)	0.3939
T_{max}	min	2.00 (0.21)[b]		1.00 (0.00)	0.0022[b]
CL_z	L min^{-1} ppbv^{-1}	59.33 (16.05)	L kg^{-1}	0.08 (0.02)	—
C_{max}	ppbv	11.09 (6.80)	μg L^{-1}	11307.66 (2775.73)	—
MRT (0–t)	min	7.82 (2.45)		4.73 (1.13)	0.0931
MRT (0–∞)	min	10.55 (4.94)		8.47 (2.92)	0.5887
λ_z	min^{-1}	0.15 (0.14)	min^{-1}	0.09 (0.05)	0.5128

[a] NCA, non-compartment model; the subscript 'z' indicates that the analysis data results are from a non-compartment model. Data of PK parameters were expressed as mean (SD). $C_{exhaled}$, propofol concentration in exhaled air; C_{plasma}, propofol concentration in plasma; AUC, area under the curve; R_AUC (t/∞), corrected area under the curve; $T_{1/2}$, half-life; CL_z, apparent clearance; C_{max}, peak concentration; MRT, mean residence time; λ_z, slope of the terminal phase regression line; —, solid horizontal line represents that the indicators are not comparable due to differences in units of measurement. [b] $P < 0.05$ with T_{max} from C_{plasma}.

(Shanghai, China) and are presented as arithmetic means (SD) in Table 2. Among the parameters derived from $C_{exhaled}$ and C_{plasma}, only T_{max} (time to peak concentration) showed a significant difference. The peak $C_{exhaled}$ occurred at 2.00 ± 0.21 min, significantly later than the peak C_{plasma} at 1.00 ± 0.00 min.

Although the area under the curve (AUC) values of drug concentration over time for $C_{exhaled}$ and C_{plasma} are not directly comparable due to dimensional differences, the R_AUC (t/∞) values exceeded 80% in both cases, indicating that both concentration forms adequately reflect the *in vivo* processes of absorption, distribution, metabolism, and excretion. Mean Residence Time (MRT) is an important parameter describing the residence time of a drug in the body, reflecting the total time required for the processes of absorption, distribution, and elimination of the drug. MRT (0–t) and MRT (0–∞) derived from $C_{exhaled}$ (7.82 ± 2.45 min, 10.55 ± 4.94 min) were higher than those from C_{plasma} (4.73 ± 1.13 min, 8.47 ± 2.92 min), but the differences were not statistically significant ($P = 0.0931$ and $P = 0.5887$). Similarly, the elimination rate constants (λ_z) for $C_{exhaled}$ (0.15 ± 0.15 min^{-1}) and C_{plasma} (0.09 ± 0.05 min^{-1}) showed no significant difference ($P = 0.5128$).

4 Discussion

This study is a preclinical investigation, requiring comprehensive validation of UV-TOF MS technology. Beagle dogs were chosen for their anatomical and physiological similarity to humans.[20] Young Beagles (1.5–2 years old) offer stable body weight and physiological states, sufficient tidal volume for analysis, and minimal variability in exhaled breath components, making them ideal for repeated studies. Standard anesthesia and breath sampling procedures are well tolerated, and unlike smaller animals, Beagles recover fully without long-term effects.

UV-TOF MS is a highly efficient mass spectrometry technique that eliminates the need for sample preprocessing or parameter optimization. Its key advantage lies in a high-efficiency ion analyzer, enabling high-throughput and simultaneous analysis of multiple molecules. Signal accumulation depends on acquisition time, with longer durations enhancing signal strength. In this study, a 20-second acquisition time and a gas sampling flow rate of 70 mL min^{-1} were used for exhaled air analysis. The method demonstrated excellent linearity, with a calibration curve spanning 3.23 to 46.13 ppbv ($R^2 = 0.9939$), covering the reported clinically relevant propofol range by 0–20 ppbv (ref. 21) and 2–39 ppbv,[22] thereby meeting clinical requirements. Accuracy and repeatability were confirmed through intra- and inter-day precision analyses, with the imprecision values remaining below 15% across different propofol concentrations.

Carry-over effects were minimized to within 10%. Unlike previous studies reporting propofol adhesion in detection systems,[23] our results indicate rapid clearance within the UV-TOF MS system. This is likely due to two factors: the use of polyether ether ketone (PEEK) sampling tubes and gas pipelines with minimal surface adsorption,[24] and the high-vacuum operation (500 ± 20 Pa) system, which efficiently absorbs and expels gaseous compounds, preventing accumulation.

The matrix effect was not investigated, as ultraviolet photoionization, a soft ionization technique, minimizes polarity discrimination, ion suppression, and matrix interference, enabling real-time trace analysis without pretreatment. A direct-current krypton lamp (10.6 eV) ionizes analytes in a high-vacuum environment, producing minimal fragment ions when photon energy exceeds the analyte's ionization threshold ($M + h\nu \rightarrow M^+ + e^-$). The ionization energies of common air components—N_2 (15.58 eV), CO_2 (13.77 eV), O_2 (12.07 eV), and H_2O (12.62 eV)—exceed the UV photon energy, preventing ionization and minimizing interference. This reduces moisture impact in exhaled air, eliminating the need for matrix-matched propofol standards. UV-TOF MS enables direct gas analysis with low sample consumption, high sensitivity, and no pretreatment.

Calibrating gaseous propofol is challenging due to its low solubility and volatility. While previous studies used organic solvents like methanol or ethanol to dissolve propofol, followed by dilution in water,[25,26] the low exhaled propofol concentrations (ppbv range) make its 124 mg per L water solubility sufficient. This study prepared an aqueous stock solution below the solubility limit of propofol, ensuring adequate dissolution. Calibration confirmed that aqueous solution provides accurate, reproducible measurements without organic co-solvents, validating feasibility.

After the bolus injection of propofol, a moderately strong correlation ($R^2 = 0.7950$) was observed between $C_{exhaled}$ and C_{plasma}. This result is consistent with findings by Lukas *et al.*, who reported a similar correlation ($R^2 = 0.71$) in rats.[14] As an exploratory study, this correlation highlights the potential for using exhaled propofol concentrations to predict plasma levels. Overall PK profiles for both $C_{exhaled}$ and C_{plasma} follow similar pharmacokinetic trends, adequately reflecting *in vivo* absorption, distribution, metabolism, and excretion processes, as indicated by (R_AUC > 80%). While AUC values are not directly comparable due to dimensional differences, both measures capture drug exposure over time. MRT values for both $C_{exhaled}$ and C_{plasma} suggest a similar duration of drug retention in the body. Although MRT (0–t) and MRT (0–∞) were higher for $C_{exhaled}$, these differences were not statistically significant ($P = 0.0931$ and $P = 0.5887$). The λ_z for $C_{exhaled}$ and C_{plasma} showed no significant difference ($P = 0.5128$), indicating similar elimination kinetics.

Nevertheless, a delay in T_{max} for $C_{exhaled}$ (2.00 ± 0.21 min) was observed compared to C_{plasma} (1.00 ± 0.00 min, $P < 0.05$), possibly due to the substantial blood/air partition coefficient of propofol and redistribution or transit time through the pulmonary system. Actually, the UV-TOF MS system could immediately detect the presence of propofol when the corresponding standard gas was introduced, indicating that these delays were not caused by adsorption on the instrument pipelines. It takes a certain time to achieve equilibrium between free propofol in the blood and volatile gaseous propofol in the breath.[27,28] Additionally, conditions such as alveolar membrane diseases or hemodynamic fluctuations may exacerbate the

delayed peak intensity of exhaled propofol.[29] While not statistically significant, the higher MRT (0–t) and MRT (0–∞) values for $C_{exhaled}$ (7.82 ± 2.45 min and 10.55 ± 4.94 min) compared to C_{plasma} (4.73 ± 1.13 min and 8.47 ± 2.92 min) also suggest a longer persistence of propofol in exhaled breath, possibly due to delayed pulmonary clearance or continuous release from systemic circulation. To address this, we further investigated the correlation between exhaled propofol concentration and its anesthetic effect. The relationship with the BIS value showed a moderate fit to a one-phase exponential decay model (R^2 = 0.5501), indicating the potential of real-time exhaled propofol monitoring to guide titration and maintain sedation. This finding underscores its significant clinical relevance for anesthesia management.

This study has limitations. First, inaccuracies in gaseous propofol concentrations may arise from its semi-volatile nature, deviating from ideal volatile compound behavior. Second, BIS monitoring, used as a surrogate for sedation depth, showed only moderate correlation with exhaled propofol, limiting its clinical applicability. Previous studies[30] caution against using BIS for anesthetic depth in dogs, as its algorithm was designed for humans. In Beagles, this moderate correlation may result from the lack of a species-specific BIS algorithm, with factors like posture and movement further affecting reliability.

To overcome these limitations, further studies should incorporate advanced EEG-derived measures, such as the patient state index, burst suppression ratio, spectral edge frequency (95%), and density spectral array,[31,32] for more precise differentiation of propofol-induced unconsciousness in dogs. Combining these methods with BIS monitoring could enhance sedation assessment and support real-time exhaled propofol monitoring. Given interspecies differences, clinical trials are needed for validation beyond animal studies.

A key challenge in continuous exhaled breath collection is the inability to distinguish between exhalation and inhalation phases and to eliminate anatomical dead space effects. While we have investigated dead space influence,[33] inhalation introduces gases (*e.g.*, room air or oxygen) into the sampling system, diluting target compounds like propofol and leading to lower measured concentrations than in exhaled breath.

In this study, canine respiratory parameters were maintained at a tidal volume of 10 mL kg^{-1}, respiratory rate of 20 breaths per minute, and an inhalation-to-exhalation ratio of 1 : 2. This ratio indicates that two-thirds of the respiratory cycle is exhalation, suggesting that approximately two-thirds of the collected gas originates from exhaled breath, while one-third is influenced by inhaled air dilution. Since gas composition differs between phases, continuous sampling causes signal fluctuations, with higher target compound concentrations during exhalation and lower or near-zero levels during inhalation. These fluctuations affect data stability and repeatability, complicating analysis.

However, as a direct mass spectrometry technique, UV-TOF MS used in our study integrates all detected components over a sampling period, where longer collection times yield higher signal intensities. The UV-TOF MS system can complete ionization and detection within 0.1–60 s. In this work, we used a 20 s acquisition time with about 70 mL min^{-1} gas to perform exhaled breath sample detection. This rapid response time may partially mitigate signal interference and no significant signal fluctuations were observed. But our future research will focus on further quantifying the impact of the dilution effect and exploring more advanced signal processing techniques to achieve more precise measurements of drug components in exhaled breath.

To mitigate these effects, scholars have made different attempts.[34,35] First is ensuring that the collected gas primarily originates from the exhalation phase. This can be achieved by using a respiratory valve or specialized sensors (*e.g.*, CO_2 monitoring sensors) or integrating respiratory monitoring devices (*e.g.*, flow meters or pressure sensors) to continuously track the respiratory cycle, ensuring that gas collection and analysis occur exclusively during exhalation. Second is employing algorithms or signal processing techniques to identify and separate exhalation and inhalation signals, allowing for the quantification and correction of dilution effects and background interference introduced during the inhalation phase. Perl *et al.* used a CO_2-controlled sample acquisition technique to provide more precise sampling and therefore more accurate breath analysis results, but there was still a delay of more than 150 ms in CO_2 data acquisition for mainstream sensors and may lead to invalid sample acquisition.[13] A study reported that human breath contains isoprene, a volatile organic compound with low inspiratory and plateau expiratory concentrations. C. Hornuss *et al.*[36,37] identified the real-time expiratory propofol signal using breath CO_2 and isoprene levels, presenting data as 30-second medians *via* ion–molecule reaction/electron impact mass spectrometry (IMR-MS). They found that isoprene measurement enables expiratory propofol detection in real-time breath monitoring, potentially simplifying CO_2 measurement. However, isoprene was measured every 1.2 seconds, about three times less frequently than CO_2, potentially reducing its precision for identifying expiratory propofol. Jiang *et al.* coupled the humidity correction in real-time with a unidirectional anisole-assisted photoionization IMS, and achieved direct breath-by-breath measurement of intraoperative propofol for the first time, which provided more clinical information for studying the anesthetic pharmacokinetics.[21]

5 Conclusions

A robust procedure for validating UV-TOF MS with a reference gas generator was successfully developed to enable online monitoring of propofol in exhaled air and was effectively validated in experiments conducted on Beagle dogs. The primary advantage of this innovative UV-TOF MS technique lies in its ability to rapidly and efficiently ionize volatile organic compounds (VOCs) without causing fragmentation, facilitating high-throughput, full-spectrum analysis. This capability ensures the precise identification of exhaled propofol and allows for the swift generation of visual spectra, providing anesthesiologists with an intuitive tool for detecting propofol in real time. The findings underscore the feasibility and potential

of UV-TOF MS as a fast, reliable, and practical method for clinical applications.

Data availability

The data supporting this article have been included as part of the ESI.†

Author contributions

CP and LXX: project administration, investigation, formal analysis, writing – original draft; ZZJ and LWW: methodology and validation; LX, KY and GDY: data curation; ZT and LJ: conceptualization, resources; ZWS: supervision, conceptualization, writing – review & editing, funding acquisition.

Conflicts of interest

The authors declare no competing financial interests or personal relationships that could have appeared to influence the work reported in this paper.

Acknowledgements

This work was supported by the NSF of China (No. 82304648), Sichuan Province Science and Technology Program (2023YFS0136), and Natural Science Foundation for Young Scientists of Sichuan Province, China (2023NSFSC1677). The authors would like to thank TopEdit (https://www.topeditsci.com/) for its linguistic assistance during the preparation of this manuscript. The authors thank Yanting Yang (ALIBEN Science & Technology Chengdu, China) for her guidance in the application of the UV-TOF MS system. The authors thank Nanfu Luo, Jing Wang, Chaoyi Deng and Linghui Yang (Laboratory of Anesthesia and Critical Care Medicine, National-Local Joint Engineering Research Centre of Translational Medicine of Anesthesiology, West China Hospital, Sichuan University) for the preparation and maintenance of laboratory equipment.

References

1 C. T. Walsh, Propofol: Milk of Amnesia, *Cell*, 2018, **175**, 10–13.
2 M. Yang and Y. Zhang, Propofol addiction: the mechanism issues we need to know, *Anesthesiol. Perioper. Sci.*, 2024, **2**, 6, DOI: 10.1007/s44254-023-00046-y.
3 I. Budic, T. Jevtovic Stoimenov, D. Pavlovic, *et al.*, Clinical Importance of Potential Genetic Determinants Affecting Propofol Pharmacokinetics and Pharmacodynamics, *Front. Med.*, 2022, **9**, 809393.
4 M. J. Devinney and M. Berger, Goldilocks and propofol dosage in older adults: too much, too little, or just right?, *J. Am. Geriatr. Soc.*, 2021, **69**, 2106–2109.
5 V. Russotto, E. Tassistro, S. N. Myatra, *et al.*, Peri-intubation Cardiovascular Collapse in Patients Who are Critically Ill: Insights from the INTUBE Study, *Am. J. Respir. Crit. Care Med.*, 2022, **206**, 449–458.
6 B. A. Baldo, Allergic and other adverse reactions to drugs used in anesthesia and surgery, *Anesthesiol. Perioper. Sci.*, 2023, **1**, 16, DOI: 10.1007/s44254-023-00018-2.
7 J. Jiang, Y. Jiao, P. Gao, *et al.*, Propofol differentially induces unconsciousness and respiratory depression through distinct interactions between GABAA receptor and GABAergic neuron in corresponding nuclei, *Acta Biochim. Biophys. Sin.*, 2021, **53**, 1076–1087.
8 F. E. Sieber, K. J. Neufeld, A. Gottschalk, *et al.*, Effect of Depth of Sedation in Older Patients Undergoing Hip Fracture Repair on Postoperative Delirium: The STRIDE Randomized Clinical Trial, *JAMA Surg.*, 2018, **153**, 987–995.
9 M. S. Avidan, L. Zhang, B. A. Burnside, *et al.*, Anesthesia awareness and the bispectral index, *N. Engl. J. Med.*, 2008, **358**, 1097–1108.
10 S. Hemphill, L. McMenamin, M. C. Bellamy and P. M. Hopkins, Propofol infusion syndrome: a structured literature review and analysis of published case reports, *Br. J. Anaesth.*, 2019, **122**, 448–459.
11 D. C. Ferrier, J. Kiely and R. Luxton, Propofol detection for monitoring of intravenous anaesthesia: a review, *J. Clin. Monit. Comput.*, 2022, **36**, 315–323.
12 X. Li, P. Martinez-Lozano Sinues, R. Dallmann, *et al.*, Drug Pharmacokinetics Determined by Real-Time Analysis of Mouse Breath, *Angew. Chem.*, 2015, **54**, 7815–7818.
13 T. Perl, E. Carstens, A. Hirn, *et al.*, Determination of serum propofol concentrations by breath analysis using ion mobility spectrometry, *Br. J. Anaesth.*, 2009, **103**, 822–827.
14 L. M. Müller-Wirtz, F. Maurer, T. Brausch, *et al.*, Exhaled Propofol Concentrations Correlate With Plasma and Brain Tissue Concentrations in Rats, *Anesth. Analg.*, 2021, **132**, 110–118.
15 T. Bruderer, T. Gaisl, M. T. Gaugg, *et al.*, On-Line Analysis of Exhaled Breath Focus Review, *Chem. Rev.*, 2019, **119**, 10803–10828.
16 Z. Wen, X. Gu, X. Tang, *et al.*, Time-resolved online analysis of the gas- and particulate-phase of cigarette smoke generated by a heated tobacco product using vacuum ultraviolet photoionization mass spectrometry, *Talanta*, 2022, **238**, 123062.
17 S. Mitschke, T. Adam and T. Streibel, Application of time-of-flight mass spectrometry with laser-based photoionization methods for time-resolved on-line analysis of mainstream cigarette smoke, *Anal. Chem.*, 2005, **77**, 2288–2296.
18 R. B. Wilson, J. C. Hoggard and R. E. Synovec, High throughput analysis of atmospheric volatile organic compounds by thermal injection – isothermal gas chromatography – time-of-flight mass spectrometry, *Talanta*, 2013, **103**, 95–102.
19 ICH Topic Q2 (R1), Validation of Analytical Procedures: Text and Methodology, *International Conference on Harmonisation*, 2005, vol. 1994, p. 17.
20 B. Hu, Recent advances in facemask devices for in vivo sampling of human exhaled breath aerosols and inhalable

environmental exposures, *TrAC, Trends Anal. Chem.*, 2022, **151**, 116600.

21 D. Jiang, C. Chen, W. Wang, *et al.*, Breath-by-breath measurement of intraoperative propofol by unidirectional anisole-assisted photoionization ion mobility spectrometry via real-time correction of humidity, *Anal. Chim. Acta*, 2021, **1150**, 338223.

22 P. R. Boshier, J. R. Cushnir, V. Mistry, *et al.*, On-line, real time monitoring of exhaled trace gases by SIFT-MS in the perioperative setting: a feasibility study, *Analyst*, 2011, **136**, 3233–3237.

23 F. Maurer, D. J. Lorenz, G. Pielsticker, *et al.*, Adherence of volatile propofol to various types of plastic tubing, *J. Breath Res.*, 2017, **11**, 016009.

24 I. D. Souza, I. G. C. Oliveira and M. E. C. Queiroz, Innovative extraction materials for fiber-in-tube solid phase microextraction: a review, *Anal. Chim. Acta*, 2021, **1165**, 238110.

25 T. Teucke, F. Maurer, L. M. Müller-Wirtz and et al., Humidity and measurement of volatile propofol using MCC-IMS (EDMON), *J. Clin. Monit. Comput.*, 2023, **37**, 493–500.

26 X. Chen, X. L. Zhang, L. Liu, *et al.*, Gas chromatograph-surface acoustic wave for quick real-time assessment of blood/exhaled gas ratio of propofol in humans, *Br. J. Anaesth.*, 2014, **113**, 807–814.

27 H. Dong, F. Zhang, J. Chen, *et al.*, Evaluating Propofol Concentration in Blood From Exhaled Gas Using a Breathing-Related Partition Coefficient, *Anesth. Analg.*, 2020, **130**, 958–966.

28 S. Dutta, Y. Matsumoto, A. Muramatsu, *et al.*, Steady-state propofol brain:plasma and brain:blood partition coefficients and the effect-site equilibration paradox, *Br. J. Anaesth.*, 1998, **81**, 422–424.

29 S. Kamysek, P. Fuchs, H. Schwoebel, *et al.*, Drug detection in breath: effects of pulmonary blood flow and cardiac output on propofol exhalation, *Anal. Bioanal. Chem.*, 2011, **401**, 2093–2102.

30 E. H. Bleijenberg, H. van Oostrom, L. C. Akkerdaas, A. Doornenbal and L. J. Hellebrekers, Bispectral index and the clinically evaluated anaesthetic depth in dogs, *Vet. Anaesth. Analg.*, 2011, **38**, 536–543.

31 C. Murillo, A. B. Weil, G. E. Moore, M. Kreuzer and J. C. Ko, Electroencephalographic and Cardiovascular Changes Associated with Propofol Constant Rate of Infusion Anesthesia in Young Healthy Dogs, *Animals*, 2023, **13**.

32 D. M. Sakai, H. N. Trenholme, F. J. Torpy, H. A. Craig and R. A. Reed, Evaluation of the electroencephalogram in awake, sedated, and anesthetized dogs, *Res. Vet. Sci.*, 2023, **159**, 66–71.

33 X. Li, P. Chang, X. Liu, *et al.*, Validation of a method for estimating pulmonary dead space in ventilated beagles to correct exhaled propofol concentration in mixed air, *BMC Vet. Res.*, 2025, **21**, 9.

34 X. Zhang, X. Ren, Y. Zhong, K. Chingin and H. Chen, Rapid and sensitive detection of acetone in exhaled breath through the ambient reaction with water radical cations, *Analyst*, 2021, **146**, 5037–5044.

35 M. Ke, H. Zhang, J. Ding, *et al.*, Generating Supercharged Protein Ions for Breath Analysis by Extractive Electrospray Ionization Mass Spectrometry, *Anal. Chem.*, 2019, **91**, 3215–3220.

36 C. Hornuss, M. E. Dolch, S. Janitza, *et al.*, Determination of breath isoprene allows the identification of the expiratory fraction of the propofol breath signal during real-time propofol breath monitoring, *J. Clin. Monit. Comput.*, 2013, **27**, 509–516.

37 C. Hornuss, D. Wiepcke, S. Praun, *et al.*, Time course of expiratory propofol after bolus injection as measured by ion molecule reaction mass spectrometry, *Anal. Bioanal. Chem.*, 2012, **403**, 555–561.

